Resonant Carbon *K*-Edge Soft X-Ray Scattering from Lattice-Free Heliconical Molecular Ordering: Soft Dilative Elasticity of the Twist-Bend Liquid Crystal Phase

Chenhui Zhu,[1,*] Michael R. Tuchband,[2] Anthony Young,[1] Min Shuai,[2] Alyssa Scarbrough,[3] David M. Walba,[3] Joseph E. Maclennan,[2] Cheng Wang,[1] Alexander Hexemer,[1,†] and Noel A. Clark[2,‡]

[1]*Advanced Light Source, Lawrence Berkeley National Laboratory, Berkeley, California 94720, USA*

[2]*Department of Physics and Soft Materials Research Center, University of Colorado Boulder, Boulder, Colorado 80309-0390, USA*

[3]*Department of Chemistry and Biochemistry and Soft Materials Research Center, University of Colorado Boulder, Boulder, Colorado 80309-0215, USA*

(Received 31 December 2015; published 7 April 2016)

Resonant x-ray scattering shows that the bulk structure of the twist-bend liquid crystal phase, recently discovered in bent molecular dimers, has spatial periodicity without electron density modulation, indicating a lattice-free heliconical nematic precession of orientation that has helical glide symmetry. *In situ* study of the bulk helix texture of the dimer CB7CB shows an elastically confined temperature-dependent minimum helix pitch, but a remarkable elastic softness of pitch in response to dilative stresses. Scattering from the helix is not detectable in the higher temperature nematic phase.

DOI: 10.1103/PhysRevLett.116.147803

The first known thermotropic liquid crystals (LCs), found by Reinitzer in 1888 [1], were the phases of cholesterol derivatives in which nematic ordering produces a well-defined mean local molecular orientation [the director field $\boldsymbol{n}(\boldsymbol{r})$] that molecular chirality drives to form a helically twisted structure [2]. This chiral nematic helix fills space with a uniform twist of $\boldsymbol{n}(\boldsymbol{r})$, with $\boldsymbol{n}(\boldsymbol{r})$ normal to the helix axis and, precessing at a constant, spatially homogeneous rate with displacement along the helix axis ($\mathbf{z}$). In 1973, Meyer realized that a homogeneous bend deformation could be added to that of the twist if helical precession of $\boldsymbol{n}(\boldsymbol{r})$ were confined to a cone rather than a plane [3], generating the heliconical nematic (HN) structure, also termed the twist-bend nematic (N_{TB}). In 2000, a theoretical proposal by Dozov [4] and simulations by Memmer [5] suggested that even in the absence of molecular chirality the bulk heliconical nematic state might, because of its bent $\boldsymbol{n}(\boldsymbol{r})$, be stabilized if made by a fluid of achiral molecules that were suitably bent-shaped. If so, the resulting N_{TB} phase would exhibit fluid, chiral conglomerate domains from achiral molecules.

Several years ago, researchers began to interpret observations on the material CB7CB [4′, 4′-(heptane-1,7-diyl)bis ([1′, 1″-biphenyl]-4″-carbonitrile), [6]] and its homologues, a class of achiral molecular dimers of rigid rods connected by a bent, flexible alkyl spacer, in terms of the heliconical nematic structure [7–13] (Fig. 1), with the isotropic (Iso), nematic (N), and the proposed HN structure of the nematic twist-bend phase appearing vs temperature T in the sequence Iso–($T = 113\,^{\circ}\mathrm{C}$)–$N$–($T = 101\,^{\circ}\mathrm{C}$)–$N_{\mathrm{TB}}$. Phases having N_{TB} characteristics have by now been observed in polar and apolar molecular dimers and trimer materials [14,15], and in bent-core mesogens [16,17]. In spite of these experimental and theoretical [18–21] developments, the structure and nature of the N_{TB} phase is not well understood, with even the proposed heliconical nematic structure still called into question [22,23]. The most direct structural evidence for the heliconical nematic structure to date has been the visualization of periodic nanoscale stripes with spacings around 80 Å on freeze-fracture planes in quenched samples [24,25]. However, NMR [22] and surface structure [23] observations have motivated recent proposals for alternative N_{TB} local structures.

An important direct, *in situ* probe of the bulk structure of an N_{TB} phase would be x-ray diffraction from its periodic planes of distinct orientational ordering. If the twist-bend helix axis is taken to be along $\boldsymbol{z}$, then its director field $\boldsymbol{n}$, giving the local mean molecular orientation, may be written as $\boldsymbol{n}(\boldsymbol{z}) = (\sin\theta\cos\varphi, \sin\theta\sin\varphi, \cos\theta)$, where θ is the heliconical tilt angle and φ is the azimuth, given by $\varphi(z) = q_H \cdot z = (2\pi/p_H)z$, where p_H is the nanoscale pitch of the helix and q_H the modulus of the corresponding wave vector. Although periodic, this proposed HN structure has heliconical glide symmetry, under a simultaneous translation δz and rotation $\varphi(\delta z)$. It therefore has no electron density modulation (EDM), and is thus not expected to produce diffraction in typical x-ray diffraction (XRD) experiments. Thus, the absence of Bragg scattering for hard (10 keV) x-ray energies, as shown in Ref. [24] and confirmed at ALS hard X-ray scattering beamline 7.3.3, is consistent with the notion that the N_{TB} phase is helical.

XRD is one of the most useful tools for characterizing the structure of LC phases because of its sensitivity to electron density modulation accompanying positional ordering [26]. However, there are modes of molecular reorientation in LCs that do not produce EDM, such as, the helical precession of the molecular tilt direction around the cone in the chiral smectic C phase of Fig. 1(c), or the alternation of molecular

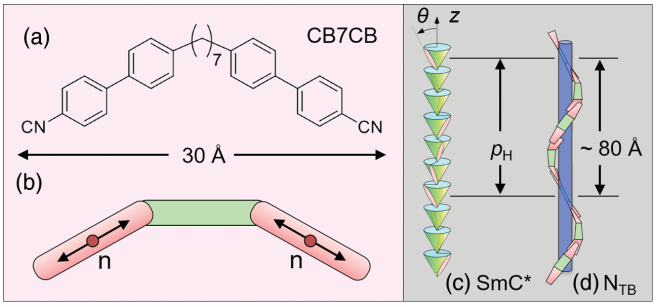

FIG. 1. (a) The dimer CB7CB consists of two cyano-biphenyl molecular arms tethered by a 7 carbon alkyl chain. (b) The molecule can be modeled as two rigid-rod segments (red) tied together by a flexible linker (green). (c) Conical helix of a chiral smectic C layered phase. (d) Proposed heliconical structure of the twist-bend (N_{TB}) phase. This molecular arrangement has helical glide symmetry and therefore no electron density modulation. It Bragg scatters x rays only near an absorption edge resonance of a constituent atom, where the cross section becomes dependent on molecular orientation. In both (c) and (d), the rigid molecular components make an average angle θ with respect to the helix axis z.

tilts in anticlinic and clock smectic phases [27]. In these cases, resonant x-ray scattering has been shown to be an effective probe of the ordering [28,29], as the coupling between linearly polarized x rays and the asymmetric electron cloud of the sample results in a tensorial atomic scattering cross section for energies near the absorption edge [30], with the scattering contrast dependent on the orientation of the molecule with respect to the polarization direction of the x-ray beam. Such experiments have generally required specially synthesized molecules doped with the target resonant atoms (Cl, S, or P), but recently carbon K-edge scattering has been applied to investigate polymer blends [31], block copolymers [32,33], organic bulk heterojunction solar cells [34], and polymeric transistors [35], in all of which the complex refractive indices of the different components have distinct energy and polarization dependences for x-ray energies near the edge. Motivated by these successes, we recently have shown that otherwise invisible helical ordering in thermotropic LCs can be observed with resonant soft x-ray scattering (RSoXS) at the carbon K edge [36] by probing the orientation of the carbon bonds in helical nanofilaments formed from bent-core molecules [37].

In this Letter, we report the use of RSoXS at the carbon K edge to provide direct evidence that the N_{TB} phase in CB7CB has a bulk helical periodic modulation of molecular orientation without modulation of electron density. We observe Bragg diffraction, peaked at wave vectors q_H, only near the carbon K-edge resonance and only at temperatures $T < 101\,^{\circ}\mathrm{C}$, the range of the N_{TB} phase and its glassy analogs at lower temperatures [38], indicative of the heliconical structure of the N_{TB} phase and enabling *in situ* measurement of its bulk helix pitch. The experiments were performed on the soft x-ray scattering beam line (11.0.1.2) at the Advanced Light Source of Lawrence Berkeley National Laboratory. The x-ray beam photon energy E was tuned between $E = 250$ eV and $E = 290$ eV in our experiments, a range including the carbon K-edge resonance at $E_R = 283.5$ eV. CB7CB was synthesized as described in the Supplemental Material [39] and filled in the isotropic phase between two pieces of 100-nm-thick Si_3N_4 membrane (Norcada, Inc.) for transmission powder diffraction study, with the sample cell and beam path in vacuum. The scattering intensity was imaged in two dimensions using a back-illuminated Princeton PI-MTE CCD, thermoelectrically cooled to $-45\,^{\circ}\mathrm{C}$, having a pixel size of 27 μm, positioned 50.6 mm down beam from the sample. The detector was translated off axis to enable recording of diffracted x-ray intensity, $I(\boldsymbol{q})$ with scattering vector $\boldsymbol{q} = \mathbf{k}_{\mathrm{scat}} - \mathbf{k}_{\mathrm{inc}}$ with q the range $q \leq 0.08$ Å^{-1} (scattering angle between $\mathbf{k}_{\mathrm{scat}}$ and $\mathbf{k}_{\mathrm{inc}}$, $\Theta \leq 32°$, $2\pi/k_{\mathrm{inc}} \sim 44$ Å). The imager then collects arcs of the diffraction rings. These rings show variations in azimuthal intensity, indicating the sample is a mosaic of domains of different size and of orientation of the N_{TB} helix. The x-ray beam (300×200 μm) is linearly polarized, with a polarization direction that can be rotated continuously from horizontal to vertical.

The RSoXS data from CB7CB are summarized in Figs. 2 and 3 and in the Supplemental Material [39], showing that distinct Bragg scattering rings, indicating a periodic bulk lamellar structure at wave vectors in the range 0.06 Å$^{-1} < q_H < 0.08$ Å^{-1}, appear in CB7CB for $T < 101\,^{\circ}\mathrm{C}$ and $E \sim E_R$. At $T = 25\,^{\circ}\mathrm{C}$ this scattering appears as a well-defined ring at $\Theta_H \sim 32°$, corresponding to $q_H = 0.78$ Å^{-1} and indicative of a lamellar structure of period $p_H = 2\pi/q_H = 80.6$ Å. The 2D arcs $I(\boldsymbol{q})$, such as shown in Figs. 2(a)–2(f), are azimuthally averaged around the beam center $\boldsymbol{q} = 0$, over the observable angular range that depends on q, to obtain the 1D radial scans $I(q)$ plotted in Fig. 2(g). The detailed structure of the detected rings indicates that the scattering originates from a powderlike mosaic of domains that are internally well ordered but distributed in azimuthal orientation, size, and peak position q. Bragg scattering is detectable for E only in the range 266 eV $< E < 287$ eV, with a sharp maximum in peak area $A(E)$ at $E_R = 283.5$ eV, the energy used for the runs vs temperature (T) that gave the temperature data in Fig. 2 and the Supplemental Materials. The peak disappears into the background with increasing $|E - E_R|$ (see Supplemental Material, Fig. 1 [39]). For $E > E_R$ this is due in part to the large step in sample attenuation at $E = E_R$ (Supplemental Material, Fig. 2 [39]). However, for $E < E_R$ it indicates the decay of the Bragg scattering cross section, since at lower E the loss of Bragg intensity due to absorption is limited to ~30% or less. Near the $N - N_{TB}$ transition we find $q_H \sim 0.064$ Å^{-1} ($p_H \sim 98$ Å), comparable to the periodicity measured by FFTEM [24,25] and estimated from electroclinic measurements [52]. These observations indicate that the scattering from CB7CB is due to a helical nematic structure, the only way to generate

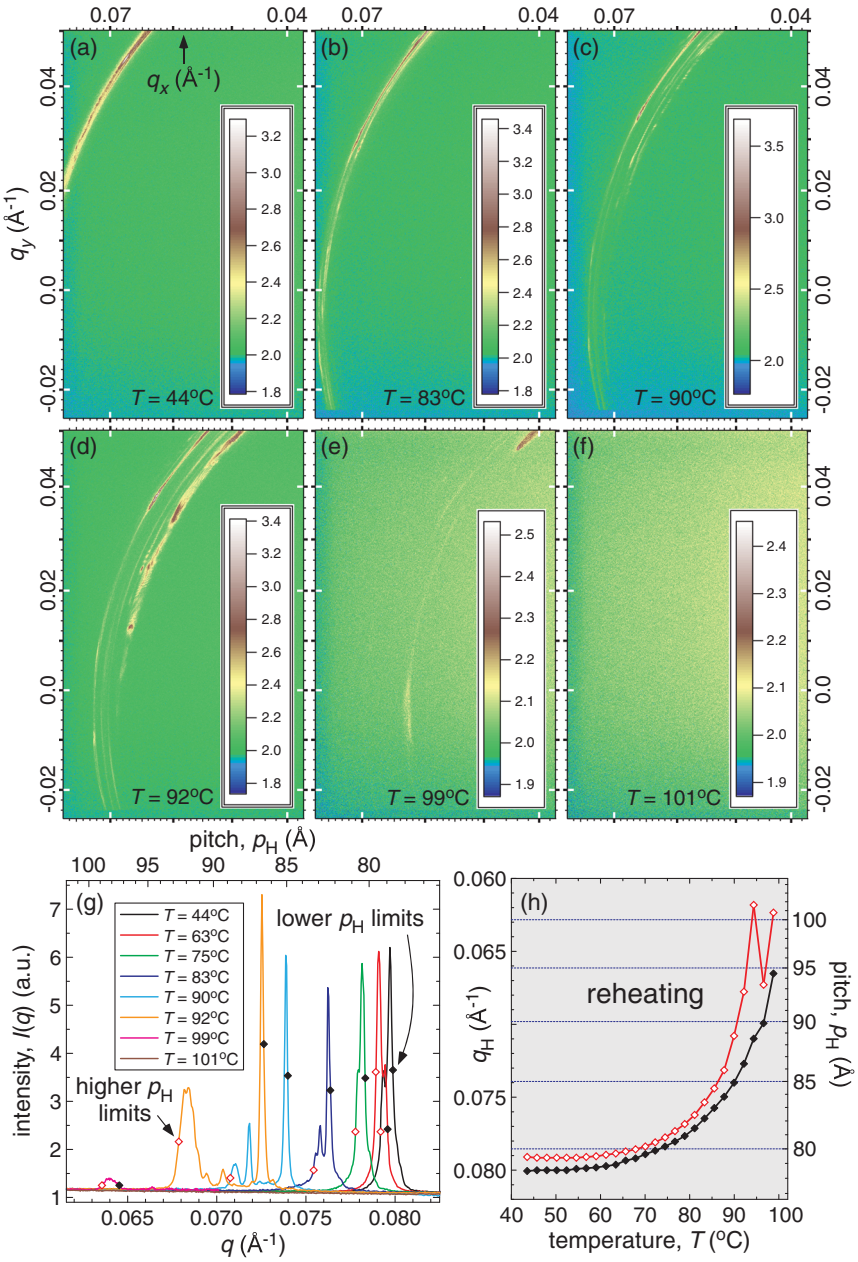

FIG. 2. (a)–(f) RSoXS, with incident x-ray photon energy at the carbon K edge ($E = 283.5$ eV), of the twist-bend nematic phase of CB7CB as a function of temperature on reheating, after heating into the nematic and cooling to $T = 25\,°C$. The scattering arcs generally broaden and shift to smaller q as T increases, corresponding to a mosaic of N_{TB} domains with a variety of pitch lengths that reach up to ~100 Å at temperatures near the $N - N_{TB}$ transition. (f) There is no observable scattering in the higher temperature nematic phase. (g) Radial scans in q of azimuthal averages of $I(\boldsymbol{q})$ about the beam center $q = 0$ of the images in (a)–(f), each for the entire available range of φ. The limits of the pitch distribution are measured from the half maximum of the outermost scattering peaks, with the upper p_H limit denoted by the open red diamonds and the lower p_H limit by closed black diamonds. (h) Higher and lower limits of q_H and p_H as measured from line scans which include the entire scattering arc. At high temperatures the trend in the lower limit of p_H is significantly smoother than the higher limit, implying that the lower p_H limit represents the strain-free pitch of CB7CB.

resonant Bragg diffraction in the absence of EDM, and that the scattering cannot be accounted for by proposed local nanostructures that are either not periodic [22] or which have EDM [22,23] (see discussion in the Supplemental Material [39]). Furthermore, the positive birefringence of the N_{TB} phase, comparable in sign and magnitude to that of the nematic [24], indicates that $\theta < 54.7°$, the magic angle, ruling out any cholesteric-like helix having $\theta = 90°$, and leaving the heliconical nematic as the only remaining possible structure. In this case, since the geometries for $\varphi = \pi$ and $\varphi = 2\pi$ are distinct, the lowest-order resonant Bragg scattering is at $q_H = 2\pi/p_H$, where p_H is the full helix pitch, the distance along $\mathbf{z}$ for a $\varphi = 2\pi$ rotation around the cone [Fig. 1(d)].

The RSoXS technique has enabled the first *in situ* studies of the bulk heliconical nematic structure and pitch as a function of temperature, with the results of a heating-cooling-reheating cycle (between $T = 25\,°C$ and the nematic phase) shown in Figs. 2 and 3 (see Supplemental Material [39]). This series of measurements started from $T = 25\,°C$ with a sample previously melted into the Iso phase and cooled to room temperature in order to fill the cell. For the heating scans $I(\boldsymbol{q}, T)$ at low T is generally a single ring as in Fig. 2(a), but, remarkably, broadens with increasing T into a pattern of distinct arcs, each a partial ring localized in q but with a finite range of azimuthal orientations, as shown in Figs. 2(c) and 2(d).

At higher T in the N_{TB}, the scattering is a superposition of distinct peaks at different q_H values [Figs. 2(c)–2(e)],

some quite sharp. The half-width at half maximum (HWHM) of the narrowest of these is found to be $\delta q_H \sim 2 \times 10^{-4}$ Å^{-1}. This width is comparable to the intrinsic resolution of the scattering geometry, $\delta q_{\rm res} = k_{\rm inc} \cos(\Theta/2) \cos^2\Theta (w/L) \sim 2 \times 10^{-4}$ Å^{-1} HWHM, limited by the width of the beam, $w \sim 200$ μm, and $L = 50.6$ mm the sample to detector separation, indicating that the scattering from single domains can be nearly resolution limited, even for T close to the $N - N_{\rm TB}$ transition. Since $\delta q_{\rm res}$ corresponds to the coherence length in the scattering of $l = \delta q_{\rm res}^{-1} \sim 1$ μm, the single peak width shows that the domains can be locally well ordered over micron scale volumes, corresponding to coherent ordering over >100 periods of the periodic lamellar structure, consistent with the FFTEM images of micron-scale areas [24,25]. The broader peaks may indicate local order with a more limited range of layer correlation or the presence of several domains of differing peak position.

The spread in peak positions at a given T implies a distribution of pitches $P(p_H)$, characterized in Figs. 2(g) and 2(h) by plotting the higher and lower limits of pitch p_H at each temperature for the heating and cooling scans. The width of the distribution of pitches, Δp_H, is narrowest at low T, where $\Delta p_H / p_H \sim 0.35/80 = 0.0044$, and increases to a maximum of $\Delta p_H / p_H \sim 8.6/93 = 0.093$ as the transition to the nematic is approached. The width $\Delta p_H T$ then decreases over the phase coexistence range of a few degrees near the transition [vertical cyan bar in Figs. 3(d)–3(f)], as the smaller peaks transition into the nematic, a process completed by the disappearance of the last single peak to give no detectable Bragg scattering in the nematic phase, a behavior indicative of a first-order transition.

Plots of the individual temperature scans in Figs. 3(a)–3(c) show the distinct broadening of the pitch distribution with increasing T and upon cooling the corresponding shrinking to a single peak or a narrow distribution of peaks. In each case, the variation in the value of the higher p_H limit, $p_H(T)_{\rm high}$, is much larger and more erratic than that of the lower limit, $p_H(T)_{\rm low}$. Superposition of the higher and lower limit data in Figs. 3(d)–3(f) shows that, in fact, $p_H(T)_{\rm low}$ exhibits very little variation among the three runs, the principal deviation among them being a shift of $p_H(T)$ to lower temperatures by ~1 °C relative to the heating curves near the $N - N_{\rm TB}$ transition, due the hysteresis of the transition on cooling vs heating. This constancy of $p_H(T)_{\rm low}$, also evident in typical families of multipeak structures obtained by taking a series of azimuthal averages over narrow azimuthal sectors (Supplemental Material, Fig. 5 [39]), can be taken as evidence that $p_H(T)_{\rm low}$ is, in fact, the strain-free pitch of the $N_{\rm TB}$ in CB7CB. In CB7CB on heating, the strong expansion of the pitch must mean that the helix is under varying degrees of local compressive stress. While domains with varying degrees of expansion of the pitch appear, there are none showing up with the pitch

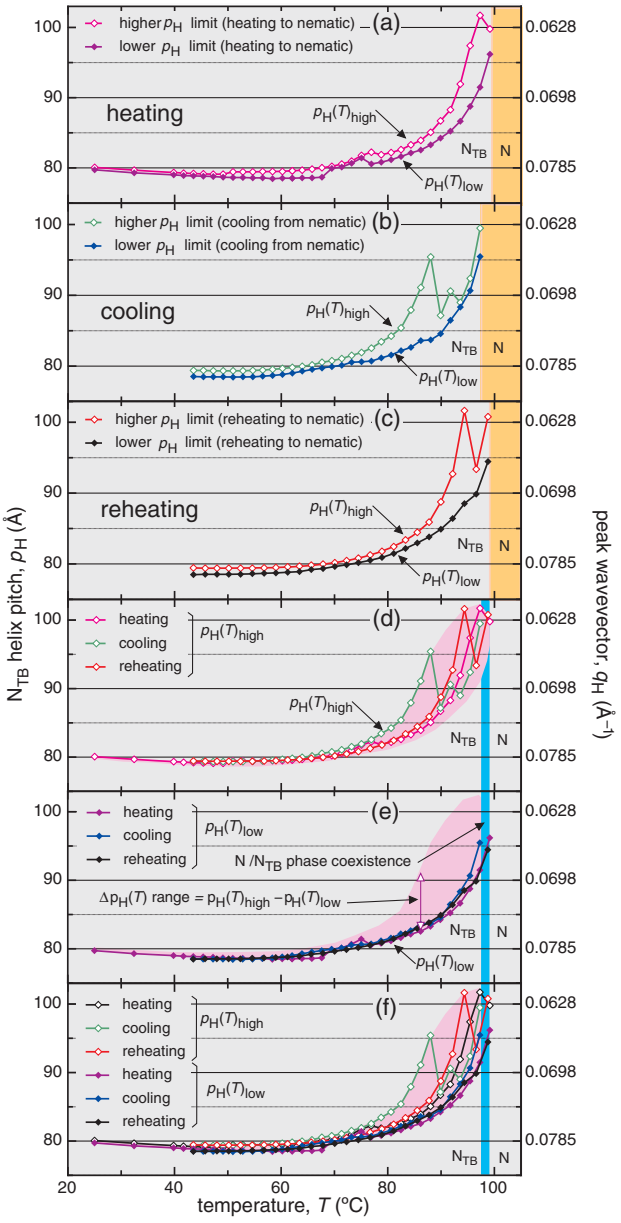

FIG. 3. (a)–(c) CB7CB pitch range limits as a function of temperature on initial heating (a), cooling (b), and reheating (c), measured from Fig. 2 and Supplemental Material, Figs. 3 and 4 as described in the caption of Fig. 2. The orange shaded region indicates the temperature interval of the nematic phase, where no RSoXS is observed, and shows hysteresis upon heating vs cooling. (d)—(f) Plots combining the higher (d), lower (e), and all (f) p_H limit data from the three temperature scans. The purple-pink shading shows $\Delta p_H(T) = p_H(T)_{\rm high} - p_H(T)_{\rm low}$, the range of measured pitch lengths indicated by the data. The width of the vertical cyan bar denotes the temperature interval over which there is $N_{\rm TB}/N$ phase coexistence.

substantially compressed. This implies that the elastic energy required to change a pitch is very asymmetric at higher temperatures in the $N_{\rm TB}$ phase, with the stress required for a certain fractional dilation being much smaller than that for compression. An additional feature to be pointed out is that

during the cooling run the N_{TB} appears at $T \sim 100\,°C$ as a single peak located on the lower limit curve, a further indication that the lower limit curve is giving nearly strain-free pitch values since isolated N_{TB} domains are likely to be strain free.

The broad distribution $P(p_H)$ of sharp peaks indicates the presence of domains that have homogeneous internal strain induced by an inhomogeneous distribution of varying, local stresses. An estimate of the form of the elastic energy determining the pitch, $U(p_H)$, has been made by assuming that these local stresses are randomly distributed and that $U(p_H) \propto -C \ln[P(p_H)]$, where C is an unknown measure of the rms stress fluctuation (Supplemental Material, Fig. 7 [39]). Softening of $U(p_H)$ for layer dilation at high T is evident. Many of these peaks in $I(q)$ come from rings in $I(\boldsymbol{q})$ that extend in the images over many tens of degrees in azimuthal angle ϕ, indicative of curved structures with a certain pattern of pitch dilation everywhere, perhaps in focal conic domains, which are commonly seen in the HN phase [12]. However, an optical microscopy study of such structures shows that, once formed, they tend to persist upon cooling and are thus likely present at the lower temperatures. In this case, the collapse of the distribution of p_H to a narrow range of values would have to be due to an elastic resistance to pitch dilation that increases with decreasing temperature (see discussion in the Supplemental Material [39]).

We acknowledge the use of beam lines 11.0.1.2 and 7.3.3 of the Advanced Light Source supported by the Director of the Office of Science, Office of Basic Energy Sciences, of the U.S. Department of Energy under Contract No. DE-AC02-05CH11231. This work was supported by the Soft Materials Research Center under NSF MRSEC Grant No. DMR-1420736.

*Corresponding author.
chenhuizhu@lbl.gov
†Corresponding author.
ahexemer@lbl.gov
‡Corresponding author.
noel.clark@colorado.edu

[1] F. Reinitzer, Monatsh. Chem. **9**, 421 (1888).
[2] M. F. Grandjean, Academie Serbe des Sciences et des Arts, Glas, Classe des Sciences Techniques **172**, 71 (1921).
[3] R. B. Meyer, in *Molecular Fluids*, edited by R. Balian and G. Weil (Gordon and Breach, New York, 1976), pp. 273–373.
[4] I. Dozov, Europhys. Lett. **56**, 247 (2001).
[5] R. Memmer, Liq. Cryst. **29**, 483 (2002).
[6] P. J. Barnes, A. G. Douglass, S. K. Heeks, and G. R. Luckhurst, Liq. Cryst. **13**, 603 (1993).
[7] V. P. Panov, M. Nagaraj, J. K. Vij, Y. P. Panarin, A. Kohlmeier, M. G. Tamba, R. A. Lewis, and G. H. Mehl, Phys. Rev. Lett. **105**, 167801 (2010).
[8] L. Beguin, J. W. Emsley, M. Lelli, A. Lesage, G. R. Luckhurst, B. A. Timimi, and H. Zimmermann, J. Phys. Chem. B **116**, 7940 (2012).
[9] M. Cestari, E. Frezza, A. Ferrarini, and G. R. Luckhurst, J. Mater. Chem. **21**, 12303 (2011).
[10] P. A. Henderson and C. T. Imrie, Liq. Cryst. **38**, 1407 (2011).
[11] V. P. Panov, R. Balachandran, M. Nagaraj, J. K. Vij, M. G. Tamba, A. Kohlmeier, and G. H. Mehl, Appl. Phys. Lett. **99**, 261903 (2011).
[12] M. Cestari, S. Diez-Berart, D. A. Dunmur, A. Ferrarini, M. R. de la Fuente, D. J. B. Jackson, D. O. Lopez, G. R. Luckhurst, M. A. Perez-Jubindo, R. M. Richardson, J. Salud, B. A. Timimi, and H. Zimmermann, Phys. Rev. E **84**, 031704 (2011).
[13] V. P. Panov, R. Balachandran, J. K. Vij, M. G. Tamba, A. Kohlmeier, and G. H. Mehl, Appl. Phys. Lett. **101**, 234106 (2012).
[14] Y. Wang, G. Singh, D. M. Agra-Kooijman, M. Gao, H. K. Bisoyi, C. Xue, M. R. Fisch, S. Kumar, and Q. Li, CrystEngComm **17**, 2778 (2015).
[15] S. M. Jansze, A. Martínez-Felipe, J. M. D. Storey, A. T. M. Marcelis, and C. T. Imrie, Angew. Chem., Int. Ed. **54**, 643 (2015).
[16] D. Chen, M. Nakata, R. Shao, M. R. Tuchband, M. Shuai, U. Baumeister, W. Weissflog, D. M. Walba, M. A. Glaser, J. E. Maclennan, and N. A. Clark, Phys. Rev. E **89**, 022506 (2014).
[17] M. W. Schröder, S. Diele, G. Pelzl, U. Dunemann, H. Kresse, and W. Weissflog, J. Mater. Chem. **13**, 1877 (2003).
[18] E. G. Virga, Phys. Rev. E **89**, 052502 (2014).
[19] C. Meyer and I. Dozov, Soft Matter **12**, 574 (2016).
[20] C. Greco and A. Ferrarini, Phys. Rev. Lett. **115**, 147801 (2015).
[21] G. Barbero, L. R. Evangelista, M. P. Rosseto, R. S. Zola, and I. Lelidis, Phys. Rev. E **92**, 030501 (2015).
[22] A. Hoffmann, A. G. Vanakaras, A. Kohlmeier, G. H. Mehl, and D. J. Photinos, Soft Matter **11**, 850 (2015).
[23] E. Gorecka, M. Salamonczyk, A. Zep, D. Pociecha, C. Welch, Z. Ahmed, and G. H. Mehl, Liq. Cryst. **42**, 1 (2015).
[24] D. Chen, J. H. Porada, J. B. Hooper, A. Klittnick, Y. Shen, M. R. Tuchband, E. Korblova, D. Bedrov, D. M. Walba, M. A. Glaser, J. E. Maclennan, and N. A. Clark, Proc. Natl. Acad. Sci. U.S.A. **110**, 15931 (2013).
[25] V. Borshch, Y.-K. Kim, J. Xiang, M. Gao, A. Jákli, V. P. Panov, J. K. Vij, C. T. Imrie, M. G. Tamba, G. H. Mehl, and O. D. Lavrentovich, Nat. Commun. **4**, 2635 (2013).
[26] S. Kumar, *Liquid Crystals: Experimental Study of Physical Properties and Phase Transitions* (Cambridge University Press, Cambridge, 2001).
[27] H. F. Gleeson and L. S. Hirst, ChemPhysChem **7**, 321 (2006).
[28] P. Mach, R. Pindak, A.-M. Levelut, P. Barois, H. T. Nguyen, H. Baltes, M. Hird, K. Toyne, A. Seed, J. W. Goodby, C. C. Huang, and L. Furenlid, Phys. Rev. E **60**, 6793 (1999).
[29] L. S. Matkin, S. J. Watson, H. F. Gleeson, R. Pindak, J. Pitney, P. M. Johnson, C. C. Huang, P. Barois, A.-M. Levelut, G. Srajer, J. Pollmann, J. W. Goodby, and M. Hird, Phys. Rev. E **64**, 021705 (2001).
[30] A.-M. Levelut and B. Pansu, Phys. Rev. E **60**, 6803 (1999).

[31] F. Liu, C. Wang, J. K. Baral, L. Zhang, J. J. Watkins, A. L. Briseno, and T. P. Russell, J. Am. Chem. Soc. **135**, 19248 (2013).
[32] J. M. Virgili, Y. Tao, J. B. Kortright, N. P. Balsara, and R. A. Segalman, Macromolecules **40**, 2092 (2007).
[33] C. Wang, D. H. Lee, A. Hexemer, M. I. Kim, W. Zhao, H. Hasegawa, H. Ade, and T. P. Russell, Nano Lett. **11**, 3906 (2011).
[34] J. R. Tumbleston, B. A. Collins, L. Yang, A. C. Stuart, E. Gann, W. Ma, W. You, and H. Ade, Nat. Photonics **8**, 385 (2014).
[35] B. A. Collins, J. E. Cochran, H. Yan, E. Gann, C. Hub, R. Fink, C. Wang, T. Schuettfort, C. R. McNeill, M. L. Chabinyc, and H. Ade, Nat. Mater. **11**, 536 (2012).
[36] J. Stöhr, *NEXAFS Spectroscopy* (Springer, Berlin, New York, 1996).
[37] C. Zhu, C. Wang, A. Young, F. Liu, I. Gunkel, D. Chen, D. Walba, J. Maclennan, N. Clark, and A. Hexemer, Nano Lett. **15**, 3420 (2015).
[38] D. O. López, N. Sebastian, M. R. de la Fuente, J. C. Martínez-García, J. Salud, M. A. Pérez-Jubindo, S. Diez-Berart, D. A. Dunmur, and G. R. Luckhurst, J. Chem. Phys. **137**, 034502 (2012).
[39] See Supplemental Material at http://link.aps.org/supplemental/10.1103/PhysRevLett.116.147803, which includes Refs. [40–51], for some additional analysis and discussion, including off-resonance scans and additional temperature scans of CB7CB.
[40] R. J. Mandle and J. W. Goodby, ChemPhysChem (2016).
[41] A. A. Dawood, M. C. Grossel, G. R. Luckhurst, R. M. Richardson, B. A. Timimi, N. J. Wells, and Y. Z. Yousif, Liq. Cryst. **43**, 1 (2016).
[42] R. J. Mandle, C. C. A. Voll, D. J. Lewis, and J. W. Goodby, Liq. Cryst. **43**, 13 (2016).
[43] R. Mandle and J. Goodby, Soft Matter **12**, 1436 (2016).
[44] C. T. Archbold, E. J. Davis, R. J. Mandle, S. J. Cowling, and J. W. Goodby, Soft Matter **11**, 7547 (2015).
[45] K. Adlem, M. Čopič, G. R. Luckhurst, A. Mertelj, O. Parri, R. M. Richardson, B. D. Snow, B. A. Timimi, R. P. Tuffin, and D. Wilkes, Phys. Rev. E **88**, 022503 (2013).
[46] E. F. Gramsbergen, L. Longa, and W. H. de Jeu, Phys. Rep. **135**, 195 (1986).
[47] D. A. Dunmur and W. H. Miller, J. Phys. (Paris), Colloq. **40**, C3 (1979).
[48] B. R. Rajeswari, P. Pardhasaradhi, M. R. N. Rao, P. V. D. Prasad, D. M. Latha, and V. G. K. M. Pisipati, J. Therm. Anal. Calorim. **111**, 561 (2013).
[49] J. P. Jokisaari, G. R. Luckhurst, B. A. Timimi, J. Zhu, and H. Zimmermann, Liq. Cryst. **42**, 708 (2015).
[50] C. Meyer, G. R. Luckhurst, and I. Dozov, J. Mater. Chem. C **3**, 318 (2015).
[51] M. R. Tuchband, M. Shuai, K. A. Graber, D. Chen, L. Radzihovsky, A. Klittnick, L. Foley, A. Scarbrough, J. H. Porada, M. Moran, E. Korblova, D. M. Walba, M. A. Glaser, J. E. Maclennan, and N. A. Clark, arXiv:1511.07523.
[52] C. Meyer, G. R. Luckhurst, and I. Dozov, Phys. Rev. Lett. **111**, 067801 (2013).